

Magnetization waves in split-ring-resonator arrays: Evidence for retardation effectsManuel Decker,^{1,2} Sven Burger,^{3,4} Stefan Linden,^{1,2} and Martin Wegener^{1,2}¹*Institut für Angewandte Physik and DFG-Center for Functional Nanostructures (CFN), Universität Karlsruhe (TH), D-76128 Karlsruhe, Germany*²*Institut für Nanotechnologie, Forschungszentrum Karlsruhe in der Helmholtz-Gemeinschaft, D-76021 Karlsruhe, Germany*³*Zuse Institute Berlin, Takustrasse 7, D-14195 Berlin, Germany*⁴*DFG Forschungszentrum Matheon, Strasse des 17. Juni 136, D-10623 Berlin, Germany*

(Received 18 September 2009; published 5 November 2009)

We excite low-symmetry planar arrays of nanoscale magnetic split-ring resonators oscillating at around 200 THz frequency under oblique incidence of light. Due to the in-plane coupling of split-ring resonators, classical magnetic-dipole waves result in the plane. We measure the dispersion relation of “antiferromagnetic” and “ferromagnetic” modes, revealing backward waves and a wave-vector-dependent damping. The latter provides evidence for retardation effects, which play no role in the quantum-mechanical counterpart of classical magnetization waves, i.e., magnons. Our experiments are in good agreement with both simple heuristic modeling and microscopic theory.

DOI: [10.1103/PhysRevB.80.193102](https://doi.org/10.1103/PhysRevB.80.193102)

PACS number(s): 42.25.Bs

A split-ring resonator (SRR) is a tiny resonant electromagnet into which the incident light field can induce a circulating and oscillating electrical current, leading to a magnetic-dipole moment perpendicular to the SRR plane.¹ Thus, SRR can be viewed as the classical analog of magnetic-dipole moments connected with quantum-mechanical orbital angular momentum or spin. For SRR on the nanometer scale, the SRR resonance lies in the optical frequency range.^{2–4} If many SRR are densely packed into an artificial material (a “metamaterial”), the interaction among the SRR can become important^{5–10}—just like the interaction of the magnetic-dipole moments of quantum-mechanical orbital angular momenta or spins is crucial in usual ferromagnetic or antiferromagnetic materials.¹¹

Apart from these similarities, there are also obvious fundamental differences between classical SRR and quantum-mechanical spins (or, likewise, quantum-mechanical orbital angular momenta): (i) spins exist on their own, whereas the SRR magnetic-dipole moment disappears as soon as the light field is switched off. (ii) The spin magnetic-dipole moment can be static, the SRR magnetic-dipole moment necessarily oscillates (here beyond 200 THz frequency). Thus, when we use the notions “antiferromagnetic” or “ferromagnetic” for SRR in this Brief Report, we exclusively refer to *snapshots* of the SRR magnetic-dipole distribution. (iii) SRR, unlike spins, also have an electric-dipole moment. Thus, any SRR magnetic-dipole wave is always connected to an electric-dipole wave. (iv) The spin magnetic-dipole moments interact via the quantum-mechanical (indirect) exchange interaction while the SRR interact via classical electromagnetic fields—for not too small distances mainly via both their magnetic- and electric-dipole moments, for small distances via their actual electromagnetic near fields, which also comprise higher-order multipole moments beyond the dipole contributions.

In this Brief Report, we investigate the dispersion relation of in-plane antiferromagnetic and ferromagnetic magnetization waves in a low-symmetry planar SRR arrangement. Our most important finding is that not only the mode frequency but also the mode damping increases or decreases with in-

plane wave number depending on the propagation direction. This behavior indicates direction-dependent retardation effects and shows that the damping of photonic-metamaterial modes is significantly influenced by the interaction among SRR and by their relative oscillation phase.

Spin interaction, e.g., in the Heisenberg Hamiltonian, can be considered as instantaneous.¹¹ In contrast, the information propagation over a typical lattice constant, a , of a SRR array (see below) takes on the order of 1–2 fs, which is comparable to the SRR oscillation period of 5 fs at about 200 THz frequency. Hence, retardation effects can become relevant (see Ref. 12 for recent experiments on spherical metal nanoparticles). In its simplest heuristic one-dimensional classical form, this leads to the equation of motion of the magnetic-dipole moment (or some higher-order moment) $m_n(t)$ at time t and site n

$$\ddot{m}_n(t) + 2\gamma\dot{m}_n(t) + \tilde{\Omega}^2 m_n(t) = W\Omega[m_{n-1}(t-t_0) + m_{n+1}(t-t_0)]. \quad (1)$$

The dots represent the temporal derivatives. Here, we have introduced the undamped eigenfrequency $\tilde{\Omega}$, the damped eigenfrequency $\Omega = \sqrt{\tilde{\Omega}^2 - \gamma^2}$, the damping of the individual harmonic oscillators γ , the real coupling frequency W between nearest neighbors, and the retardation time delay t_0 . For time-harmonic behavior $\propto \exp(-i\omega t)$, the time delay t_0 ($t_0 \geq 0$ due to causality) translates into a phase shift $\varphi = \omega t_0 \approx \Omega t_0 = \text{const}$. The latter approximation is justified under the below conditions as the actual frequency ω will turn out to differ from Ω only by a few percent. This leads to the dispersion relation $\omega(k)$ with complex ω at real wave number k given by

$$\begin{aligned} \text{Re}(\omega) &= +\Omega - W \cos(ka) \cos(\varphi), \\ \text{Im}(\omega) &= -\gamma - W \cos(ka) \sin(\varphi). \end{aligned} \quad (2)$$

Without retardation, i.e., for $\varphi=0$, the usual¹¹ cosine-shaped magnon dispersion relation is recovered and $\text{Im}(\omega) = -\gamma$

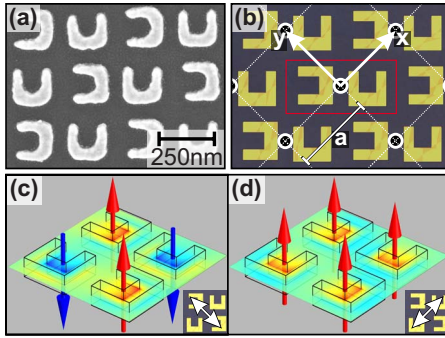


FIG. 1. (Color online) (a) Electron micrograph of the low-symmetry gold SRR array under investigation (Ref. 13). The gold thickness is 50 nm, sample footprint is $80 \mu\text{m} \times 80 \mu\text{m}$. (b) Illustration of the primitive unit cell (solid) and square lattice with lattice constant a (dashed). (c) and (d) show snapshots of axial component of the magnetic field of the (c) antiferromagnetic and the (d) ferromagnetic eigenmode that can be excited under normal incidence of light (Ref. 13).

=const. In contrast, for finite phase delays φ , the mode damping, $-\text{Im}(\omega)$, becomes k dependent. For example, for $\varphi = \pi/2$, $\text{Re}(\omega) = \Omega = \text{const.}$ while $\text{Im}(\omega)$ is dispersive. The sign of the real interaction frequency W determines whether the mode damping increases or decreases with increasing wave number k .

The SRR array under consideration is shown in Fig. 1. We have previously¹³ fabricated such gold nanostructures via electron-beam lithography and have shown by *normal-incidence* transmittance spectroscopy and comparison with theory that the system reveals two collective eigenmodes: a low-frequency antiferromagnetic and a high-frequency ferromagnetic mode. For a snapshot of the antiferromagnetic mode, the SRR magnetic-dipole components normal to the SRR plane are oriented up and down as the black and white squares on a checkerboard, whereas all point in the same direction for the ferromagnetic mode. These two eigenmodes shown in Figs. 1(c) and 1(d) can be excited by the two orthogonal linear polarizations oriented along the two diagonals. These diagonals coincide with the primitive translation vectors of the underlying square lattice that we refer to as the x and y direction in what follows [see Fig. 1(b)]. Under normal incidence of a plane wave of light, further modes can *not* be excited as all equivalent SRR in the array are driven by the same phase of the incident light field.

Investigating quantum-mechanical magnons in normal materials requires sophisticated experimental techniques such as inelastic scattering of spin-polarized neutrons¹¹ or spin-polarized electron-energy-loss spectroscopy.¹⁴ The beauty of classical magnetization waves in metamaterials is that their in-plane dispersion relation $\omega(\vec{k}_{\parallel})$ can quite easily be measured directly in an optical experiment.^{5,10} The angle of incidence β together with the free-space wavelength λ immediately allows for determination of the parallel component of the incident wave vector. It is conserved at the air-metamaterial interface hence identical with the in-plane wave vector \vec{k}_{\parallel} . This aspect is illustrated in Fig. 2. The corresponding angular eigenfrequency ω can be obtained via the resonance position in the extinction spectrum (negative loga-

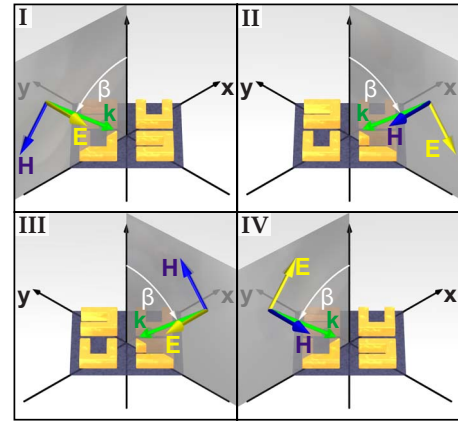


FIG. 2. (Color online) Scheme of the different geometries of oblique incidence of light investigated in this work. In each case, a certain in-plane wave-vector \vec{k}_{\parallel} results. Note that the in-plane component of the incident electric-field vector remains strictly parallel to either the x or the y direction for oblique incidence. Thus, antiferromagnetic and ferromagnetic modes are not mixed for all four depicted geometries.

rithm of the transmittance T). Selected typical measured extinction spectra are depicted in Fig. 3(a). To improve accuracy and reliability, we determine the resonance position and damping by fitting a Lorentzian to the raw data. Indeed, the above simple modeling leads to Lorentzian line shapes. Repeating this procedure for many positive and negative angles (in steps of 5° from -45° to 45° and with an opening angle

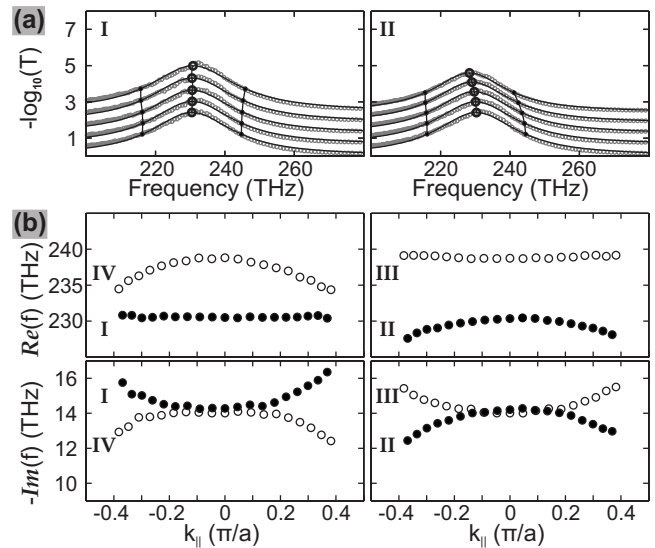


FIG. 3. (a) Selected measured extinction spectra raw data (gray) together with Lorentz fits (black). The maximum and median values of the Lorentzians are indicated by the vertical lines. The geometry corresponds to Fig. 2 (I) and (II). The angle of incidence β varies from 0° to 40° in steps of 10° (from bottom to top). These spectra are vertically displaced for clarity. (b) Dispersion relation $f(\vec{k}_{\parallel}) = \omega(\vec{k}_{\parallel})/(2\pi)$ resulting from the raw data discussed in (a) as well as the other two configurations illustrated in Fig. 2 (III) and (IV). Geometries I and IV correspond to \vec{k}_{\parallel} along x direction, II and III correspond to \vec{k}_{\parallel} along y direction.

of 5°) as well as for several polarization configurations (see Fig. 2) leads to the measured dispersion relation shown in Fig. 3(b). Here, we have plotted \vec{k}_\parallel in the first Brillouin zone of the primitive real-space unit cell that has lattice constant $a = \sqrt{2}a' = 339$ nm [see Fig. 1(b)], where a' is the SRR center-to-center spacing (note that we have previously¹³ employed a unit cell comprising four SRR that is different from the primitive one and that has had lattice constant $2a'$). Angles β up to $\pm 45^\circ$ with respect to the surface normal correspond to $|\vec{k}_\parallel| \approx 0.4 \times \pi/a$. This means that a substantial fraction of the first Brillouin zone can actually be accessed experimentally.

Starting from the low-frequency antiferromagnetic and the high-frequency ferromagnetic mode at $\vec{k}_\parallel = 0$ in Fig. 3(b), four dispersion branches result. The branches are labeled with numbers that refer to the geometries depicted in Fig. 2. Although the planar SRR array [Fig. 1(a)] has no center of inversion, all four dispersion branches show no significant asymmetry. For two of the four branches in Fig. 3(b), frequency, i.e., $\text{Re}(\omega)$, decreases with increasing modulus of the in-plane wave vector. Thus, the waves group velocity is opposite to its wave vector, hence opposite to its phase velocity, i.e., backward waves result (in the sense of $\vec{v}_{\text{phase}} \cdot \vec{v}_{\text{group}} < 0$). This aspect would lead to negative refraction at an interface in the plane of propagation. The other two dispersion branches exhibit equal direction of phase and group velocity, i.e., $\vec{v}_{\text{phase}} \cdot \vec{v}_{\text{group}} > 0$. More importantly, all four branches shown in Fig. 3(b) exhibit a dependence of the mode damping, $-\text{Im}(\omega)$, on the in-plane wave number. Following our above simple modeling, this behavior represents evidence for retardation effects. Consistent with the symmetry of the SRR array, these retardation effects depend on the direction of in-plane wave propagation and, furthermore, they are different for the antiferromagnetic and the ferromagnetic mode.

Intuitively, the overall behavior in Fig. 3(b) can be understood as follows. Suppose that electric dipole-dipole interaction dominates between adjacent primitive unit cells. For zero in-plane wave number, the total electric-dipole moment of the two SRR in each primitive unit cell for the antiferromagnetic (ferromagnetic) mode is parallel to the exciting electric-field vector and, hence, oriented along the y direction (x direction) (see Fig. 1). The antiferromagnetic mode propagating along the x direction (y direction) is a transverse (longitudinal) electric-dipole wave. Without retardation ($\varphi = 0$), it is well known that this leads to a decrease (increase) in the real part of the frequency for increasing modulus of the in-plane wave number—exactly opposite to the experimental observation in Fig. 3(b). However, following the above simple dispersion formulas, for a retardation phase φ in the interval $90^\circ < \varphi < 270^\circ$, the sign of the curvature of $\text{Re}(\omega)$ versus wave number reverses due to $\cos(\varphi) < 0$, leading to an overall agreement of this reasoning with the experimental observations in Fig. 3(b). For the ferromagnetic mode, an analogous reasoning applies but x and y direction have to be interchanged because of the orthogonal orientation of the total electric-dipole moment compared to that of the antiferromagnetic mode. This turns transverse into longitudinal waves and vice versa. Provided that the retardation phase is in the interval $90^\circ < \varphi < 180^\circ$, this reasoning also

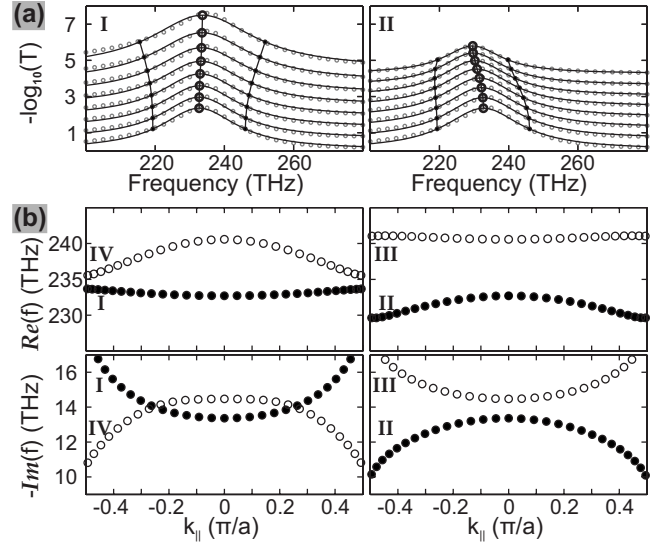


FIG. 4. (a) Selected calculated extinction spectra that can be compared directly with the experiment shown in Fig. 3(a). The angle of incidence β varies from 0° to 70° in steps of 10° (from bottom to top). (b) Resulting dispersion relation that can be compared with experiment [Fig. 3(b)].

correctly explains the curvature of the damping, $-\text{Im}(\omega)$, for all four dispersion branches. The analogous argument assuming that magnetic dipole-dipole interaction dominates between adjacent primitive unit cells does not explain the data because all dispersion branches correspond to transverse waves in this case.

Clearly, the retardation phase φ plays a crucial role in our above reasoning. To independently estimate its value, one can argue that the lattice constant of $a = 339$ nm in Fig. 1 is larger than a quarter of the free-space resonance wavelength of about $1.25 \mu\text{m}$ (equivalent to 240 THz frequency). This leads to a retardation phase exceeding 90° , perfectly consistent with our above discussion. This estimate assumes wave propagation with the vacuum speed of light. Slower propagation than that will increase the estimated retardation phase.

Note that the above reasoning based on electric dipole-dipole interaction does *not* explain the frequency splitting of the antiferromagnetic and the ferromagnetic mode at zero in-plane momentum. Magnetic dipole-dipole interactions *within* each primitive unit cell can qualitatively explain this aspect. However, interaction via higher-order multipole moments of the two nearby SRR are likely to play a role as well.

To rule out experimental artifacts and to further support our conclusions, we simulate the magnetization waves by solving Maxwell's equations for the experimental conditions. This treatment clearly includes SRR interaction via higher-order multipole moments, interaction beyond the nearest neighbors, as well as retardation effects. The sample parameters are chosen identical to those for our previous normal-incidence experiments:¹³ the lateral geometrical parameters are taken from the electron micrograph shown in Fig. 1(a), the gold thickness is 50 nm. For the description of the permittivity of gold, we use the free-electron Drude model with plasma frequency $\omega_{\text{pl}} = 2\pi \times 2108$ THz, collision frequency

$\omega_{\text{col}}=2\pi\times 24$ THz, and background dielectric constant $\epsilon_b=9.07$. The refractive index of the glass substrate is taken as $n_{\text{SiO}_2}=1.45$. We solve Maxwell's equations using a frequency-domain finite-element solver (see Ref. 10). For achieving converged results we use higher-order, vectorial finite elements and adaptive mesh refinement.

Selected numerically calculated raw data [Fig. 4(a)] and the dispersion relation [Fig. 4(b)] derived via the same procedure as described above for the experiment nicely agree with the experiment shown in Figs. 3(a) and 3(b), respectively. Importantly, the behavior of the four dispersion branches—real parts as well as imaginary parts—evolving out of the antiferromagnetic and ferromagnetic eigenmode at $\vec{k}_{\parallel}=0$ qualitatively and almost quantitatively agrees with experiment (compare Figs. 3 and 4).

In conclusion, we have discussed similarities and differences of classical and quantum-mechanical magnetization waves. While dispersive waves appear for both, we find a significant dispersion of the mode damping in the classical

case. This behavior is a retardation effect, i.e., it takes a finite time until the change in one magnetic-dipole moment arrives at an adjacent site. Depending on the relative oscillation phase between different dipoles, this effect leads to a decrease or an increase in the mode damping. Our results imply that metamaterial damping cannot only be tailored by shaping the unit cell but also by the arrangement of the unit cells onto a lattice.

ACKNOWLEDGMENTS

We thank Nils Feth and Kurt Busch's group (Karlsruhe) for discussions. We acknowledge support by the European Commission via the project PHOME and by the Bundesministerium für Bildung und Forschung via the project METAMAT. The research of S.L. is supported through a Helmholtz-Hochschul-Nachwuchsgruppe (Grant No. VH-NG-232). The graduate work of M.D. is embedded in the Karlsruhe School of Optics & Photonics (KSOP).

¹J. B. Pendry, A. J. Holden, D. J. Robbins, and W. J. Stewart, *IEEE Trans. Microwave Theory Tech.* **47**, 2075 (1999).

²S. Linden, C. Enkrich, M. Wegener, J. Zhou, T. Koschny, and C. M. Soukoulis, *Science* **306**, 1351 (2004).

³V. M. Shalaev, *Nat. Photonics* **1**, 41 (2007).

⁴C. M. Soukoulis, S. Linden, and M. Wegener, *Science* **315**, 47 (2007).

⁵M. C. K. Wiltshire, E. Shamonina, I. R. Young, and L. Solymar, *Electron. Lett.* **39**, 215 (2003).

⁶O. Sydoruk, O. Zhuromskyy, E. Shamonina, and L. Solymar, *Appl. Phys. Lett.* **87**, 072501 (2005).

⁷E. Shamonina and L. Solymar, *J. Magn. Magn. Mater.* **300**, 38 (2006).

⁸N. Liu, S. Kaiser, and H. Giessen, *Adv. Mater.* **20**, 4521 (2008).

⁹L. Solymar, E. Shamonina, and L. Solymar, *Waves in Metamaterials* (Oxford University Press, Oxford, 2009).

¹⁰G. Dolling, M. Wegener, A. Schädle, S. Burger, and S. Linden, *Appl. Phys. Lett.* **89**, 231118 (2006).

¹¹N. W. Ashcroft and N. D. Mermin, *Solid State Physics* (Harcourt College, Fort Worth, Texas, 1976).

¹²P. Olk, J. Renger, M. T. Wenzel, and L. M. Eng, *Nano Lett.* **8**, 1174 (2008).

¹³M. Decker, S. Linden, and M. Wegener, *Opt. Lett.* **34**, 1579 (2009).

¹⁴R. Vollmer, M. Etzkorn, P. S. Anil Kumar, H. Ibach, and J. Kirschner, *Phys. Rev. Lett.* **91**, 147201 (2003).